Enhancing Glioma Grading with Texture Features and SIHO-Enhanced Gradient Boosting

Thota Deepa, and Ch. D V Subba Rao

***Abstract*—Accurate grading of gliomas is critical for predicting tumor behavior and informing treatment decisions. However, traditional approaches may poorly characterize tumor heterogeneity and generally lack interpretability. In this study, we proposed an automated glioma grading framework combining de noising, hybrid segmentation, radiomic feature extraction, and LightGBM classification optimized using the Spuggy Interactive Hyperparameter Optimization (SIHO) algorithm. The novelty of SIHO is its interactive hyperparameter search mechanism, which balances exploration and exploitation to select compact and effective LightGBM hyperparameters for improved glioma grading. We built our framework on the BraTS 2019 dataset which contains a total of 335 patient cases with 259 cases of high grade glioma (HGG) and 76 cases of low-grade glioma (LGG) with T1, T1ce, T2 and FLAIR MRI modalities, as well as ground-truth masks. To improve validation rigor, both an 80:20 train-test split and k-fold cross-validation were used. Class imbalance is handled by stratified sampling and performance was assessed using accuracy, sensitivity, and specificity instead of accuracy alone. In the 80:20 evaluation, the proposed SIHO–LightGBM model achieved 96.59% accuracy, 94.73% sensitivity, and 96.98% specificity. The experimental results reveal the potential of our proposed framework for automated glioma grading.**

***Index Terms*—Glioma grading, Hybrid Feature Extraction, Light Gradient Boosting Machine, Spuggy Interactive Hyperparameter Optimization, Tumor Segmentation.**

I. Introduction

THE human brain is the central command center and a vital component of the nervous system, which plays a pivotal role in facilitating our daily activities. The brain receives sensory signals from the organs, processes these stimuli, and orchestrates decisions, ultimately transmitting instructions to the muscles. However, brain tumors are considered a critical challenge to this complex system. These tumors involve the uncontrolled growth of abnormal brain cells [1]. Among these brain tumors, gliomas are of particular concern. They are malignancies that originate from glial cells and exhibit significant h eterogeneity [2], [3]. F urthermore, g liomas display varying levels of proliferation, posing diagnostic and therapeutic challenges [4]. The World Health Organization (WHO) has classified gliomas into four distinct grades: Grade I, Grade II, Grade III, and Grade IV, which are categorized into low-grade (LGG) and high-grade gliomas (HGG) based on the malignancy and aggressive structure [5], [6]. Significant advancements in genetic profiling have led to alterations in the glioma grading and classification [7]. The classification of tumors of the central nervous system marks a departure from traditional diagnostic methods based solely on histological criteria, now incorporating molecular biomarkers [8]. In adults, more than 75% of diffuse gliomas are astrocytic, while 10% are oligodendroglial tumors [9].

Grading diffuse gliomas involves assessing histologic features such as mitotic activity [10], microvascular proliferation, and necrosis, but this task is challenging due to the tumor cell diversity, leading to significant inter observer variation [11]. Achieving progress in glioma treatment remains a challenge, and accurately grading tumor areas is crucial, especially in cases where classical surgery is risky. In such instances, safer stereotaxic biopsies and histopathological examinations are performed to determine tumor grade, enabling more informed treatment decisions [12]. Various imaging techniques have been used for glioma grading [13], [14]. Magnetic Resonance Imaging (MRI) is the desired choice for estimating intracranial tumors, and it plays a vital role in distinguishing LGG from HGG [15], [16]. However, glioma characterization using imaging is challenging because they often exhibit a mixture of LGG and HGG characteristics. Histopathological examinations, performed following surgical excision or stereotactic biopsy—often guided by MRI—continue to be the definitive method for diagnosing gliomas [17]. Machine learning (ML) techniques and deep learning models, based on MRI, have demonstrated potential in the grading of gliomas [18].

For fully automated glioma grading, it is essential to automate the selection of MRI images independently of physician supervision. This process necessitates tumor segmentation and detection preceding the grading of MRI images [31]. Furthermore, using CNNs to diagnose tumors via Whole Slide Images (WSIs) presents unique challenges due to the exceptionally high resolution, making the use of original CNNs computationally unfeasible [32]. A recent field of study, radiomics, focuses on the noninvasive decoding of tumor characteristics. Radiomics involves the extraction of extensive features to quantify tumor attributes, including scale, shape, position, intensity, and texture [2].

However, traditional radiomics methods have limitations as they extract only a restricted amount of information [21]. Various mathematical methods, ranging from simple ones

Manuscript received December 18, 2025; revised April 8, 2026. Date of publication November 5, 2026. Date of current version November 5, 2026. The associate editor prof. Matko Šarić has been coordinating the review of this manuscript and approved it for publication.

Authors are with the Department of Computer Science and Engineering, Sri Venkateswara University College of Engineering, Sri Venkateswara University, Tirupathi, Andhra Pradesh, 517502, India (e-mails: deepa.thota0607@gmail.com, subbarao chdv@hotmail.com).

Digital Object Identifier (DOI): 10.24138/jcomss-2025-0156

like linear regression and logistic regression to more intricate approaches were employed to grade gliomas [22]. While the more complex models offer greater flexibility, they also come with higher computational costs [23]. In practice, the effectiveness of the model is typically assessed through validation. For classification models, this validation process usually involves creating the model using training samples and then confirming its results using testing samples. However, due to the limited sample sizes often found in available databases, it can be challenging to perform thorough validation [24], [25], [26].

The study aims to grade the gliomas effectively using the SIHO-enabled LightGBM model. The major contributions of this study are summarized as follows:

- This study proposes a SIHO-enabled LightGBM framework for automated glioma grading through the integration of tumor segmentation, radiomic feature extraction, feature normalization, and classification.
- The proposed SIHO algorithm implements adaptive hyperparameter tuning for LightGBM by balancing exploration and exploitation through the search progression.
- A lightweight hybrid segmentation approach by combining adaptive thresholding with region growing, is used to outline tumor regions of interest and extract texture, intensity, wavelet, shape, border irregularity, and asymmetry-based radiomic features.
- The proposed framework is assessed on the BraTS 2019 dataset using an 80:20 train-test split and k-fold cross-validation. Considering the class imbalance among 259 HGG and 76 LGG cases, performance is evaluated with accuracy, sensitivity, specificity, and F1-score.

The article is organized as follows, Section II describes the literature on Glioma grading with its limitations, and Section III investigates the proposed SIHO-enabled LightGBM model. Section IV details the research results and performance analysis and the conclusions are presented in Section V.

II. Literature Review

This section explores advancements in glioma grading systems, assessing current methodologies, challenges, and emerging technologies for improved diagnostic accuracy and patient care.

Saima Rathore et.al [27] designed an SVM technique for glioma grading, by integrating multiple data sources, including clinical measures, conventional imaging, and advanced texture features, the research provides a more comprehensive and accurate prediction of glioma grades. However, the level of detail of the input image has a considerable impact on the model's accuracy. Noisy or improperly acquired MRI scans can lead to incorrect predictions. Asaf Raza et.al [28] initiated a DeepTumorNet, the model can scale to accommodate large and diverse datasets, which is crucial while dealing with medical data that may come from various sources and have variations in image quality. While the technique demonstrated high accuracy on a specific dataset, its generalizability to different populations, medical facilities, and imaging protocols needs to be further validated.

Sanghyuk et.al [29] utilized a Resnet50 V2 model for brain tumor grading, the model can automate the classification of Glioma subtypes and grading, reducing the need for manual evaluation by pathologists. This can save time and resources. Mohamed A.Naser et.al [19] used a CNN model for the detection, and grading of Glioma on MRI images to avoid the need for invasive procedures, reducing patient discomfort and risks. However, Noise, Artifacts, and variations in MRI scans can affect the segmentation and grading accuracy. Weiwei Wang et.al [20] implemented a CNN approach that can significantly minimize the time and effort essential for diagnosing and classifying gliomas, which is beneficial in clinical settings. Bing Niu et.al [30] utilized a Naive Bayes algorithm that handles multi-class categorization of brain tumors, which is more challenging but more clinically relevant than binary classification. However, the research mentions that the algorithms take a long time to process due to the extra optimization steps. This could limit its practicality in time-sensitive clinical scenarios. Building on the gaps identified in existing glioma grading approaches, the following section details the proposed SIHO-LightGBM framework for glioma grading.

III. SIHO-enabled LightGBM for Glioma Grading

Early diagnosis and grading of brain tumors is crucial for improving survival rates and lowering long-term dependencies. Nevertheless, the challenges of conventional research include a lack of diversity in datasets, restricted data availability, and potential inability to capture pertinent aspects. Furthermore, obstacles to growth in this area include interpretability concerns and the requirement for extensive validation studies. Therefore, these constraints must be addressed to develop more efficient brain tumor detection techniques. In this study, a LightGBM model is proposed for glioma grading. Initially, brain MRI scans were acquired from the BraTS 2019 database [33]. These images underwent preprocessed with Fast Non-Local Means (FNLM) denoising, followed by segmentation using a combination of adaptive thresholding and region growing algorithms. From the segmented images, a range of features are extracted, encompassing intensity-based features, texture-based features, hybrid shape-based features, wavelet transform-based features, asymmetry index, and measure of border irregularity. The extracted features are normalized because they may have different numerical ranges and scales. In this stage, all the extracted features are scaled to a common range before they are passed to the classifier. This ensures that no single feature dominates the learning process due to its larger magnitude. To grade gliomas effectively, a LightGBM classifier is employed. LightGBM hyperparameters such as numberof leaves, learning rate, maximum depth, minimum number of children and lambda_l1 are fine-tuned using the proposed SIHO algorithm, which is inspired by the communication behavior of Spuggy, a European sparrow. The block diagram of the SIHO-enabled LightGBM model is depicted in Figure 1.

A. Dataset

The experiments in this study were conducted using the BraTS 2019 dataset, a widely accessible benchmark for brain tumor analysis released through the MICCAI BraTS challenge

[33]. The training set includes 335 glioma cases, comprising 259 HGG and 76 LGG cases collected from multiple institutions. This corresponds to a class imbalance ratio of approximately 3.4:1 (HGG:LGG). Therefore, the imbalance was considered during data partitioning and evaluation using stratified sampling and by reporting sensitivity, specificity, and F1-score in addition to accuracy. Each case contains four co-registered 3D MRI modalities (T1, T1ce, T2, and FLAIR) in NIfTI (.nii.gz) format with corresponding ground-truth annotations. Since the dataset is multi-institutional and multi-modal, it provides heterogeneous imaging data suitable for evaluating automated glioma grading methods. To reduce the effect of such variability, all scans were processed using a uniform preprocessing pipeline, including co-registration, resampling to 1 mm³ isotropic resolution, skull stripping, intensity normalization, and FNLM-based denoising before segmentation and feature extraction. Although there are more recent BraTS versions, BraTS 2019 was selected as it provides explicit HGG/LGG ground-truth labels required for binary grade classification — labels removed in BraTS 2021 onward — and remains the most widely used benchmark for direct comparison with existing glioma grading literature

B. Preprocessing using Fast NLM Denoising

Fast Non-Local Means (NLM) denoising technique is utilized to remove noise from the MRI images. The Fast Non-Local Means (NLM) denoising technique enhances image quality by averaging pixel values from analogous regions within the image. This method employs a weighted sum of regions, with the weights determined by the degree of similarity between the patches. Let the noisy image be represented as I and r is the filter parameter [34].

The NLM filter working is represented with the following equation

$$\mathrm{NLM}(I)(r) = \sum_{s \in B_i} \omega(r,s)\, I(r) \tag{1}$$

where $\omega(r,s)$ is based on the pixel similarity of r and s, and ranges between 0 and 1. The similarity of pixels relies on the grayscale intensity vectors $I(M_r)$ and $I(M_s)$, where M_k represents the square of the neighborhood pixels with fixed size centered on the pixel k. This similarity can be calculated as a decreasing function of the weighted Euclidean distance $\|I(M_r) - I(M_s)\|^d_{2,d}$, where d is the standard deviation. A pixel's weight increases with similarity in gray level and decreases with differences in gray level.

$$\omega(r,s) = \frac{1}{N(r)} \exp\left(\frac{\|I(M_r) - I(M_s)\|^2_{2,d}}{L^2}\right) \tag{2}$$

The normalization constant is denoted as $N(r)$. By rapidly locating and averaging patches with similar intensity and texture characteristics, the FNLM technique preserves significant structural information while effectively minimizing noise in the image [35]. The preprocessed image is represented as B_i^*.

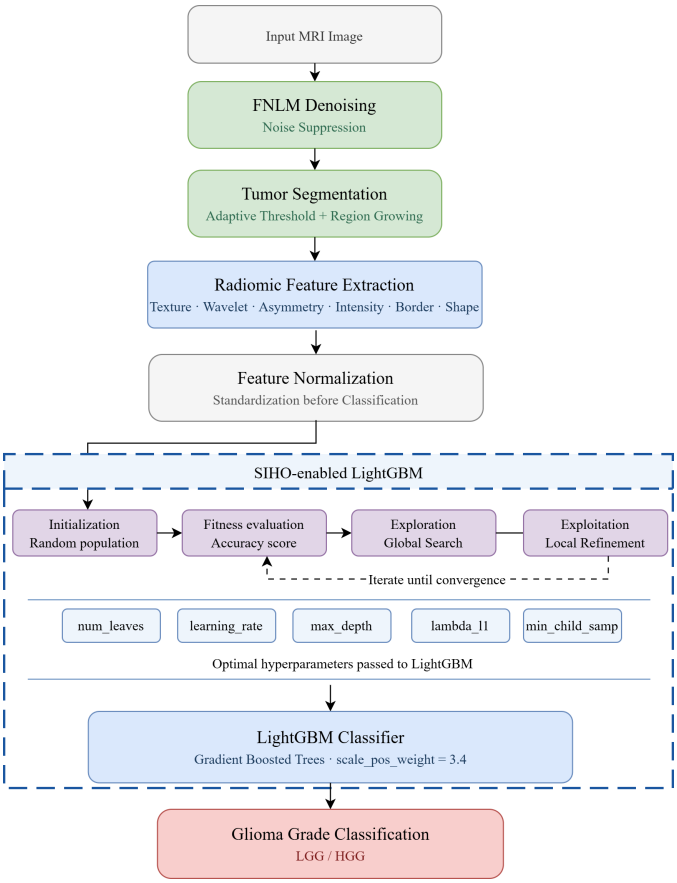


Fig. 1. Workflow of the proposed SIHO-enabled LightGBM approach for glioma grading, from image preprocessing to LGG/HGG classification.

C. Segmentation using Adaptive Thresholding and Region Growing

The integration of adaptive thresholding and region growing algorithms for glioma segmentation represents a multi-step approach in medical image analysis, designed to enhance the robustness and accuracy of models. In glioma grading systems, adaptive thresholding can be used to separate tumor regions from healthy regions [36]. Using a local threshold value for each pixel in an image based on the features of its neighborhood is the primary concept underlying adaptive thresholding, which enables improved segmentation in situations where the image intensity varies across regions.

A local neighborhood or window surrounds each pixel in the image. Depending on the application and the expected size of the items to be split, this window may have different dimensions. One possible use of the adaptive region growing algorithm is the fully automatic segmentation of medical images. Pixels that have the shortest gradient length and are not yet a component of a segmented image region are chosen as seed points in this case. The fluctuation of the gray values inside regions is thought to be smaller than the variation between regions. A size- and shape-dependent probability P_δ and a homogeneity-dependent probability P_h determine the region probability.

$$P_{\text{reg}} = P_\delta \cdot P_h \tag{3}$$

The region probability can be calculated for the tumor region based on its size, where P_δ is defined as

$$P_\delta = \begin{cases} \dfrac{\delta_2}{\delta_1}, & \text{if } \dfrac{\delta_2}{\delta_1} \leq 1, \\ 1, & \text{otherwise.} \end{cases} \tag{4}$$

After the opening process, small, thin, or highly convoluted sections are substantially smaller than large, compact regions, which change their size by just a modest amount. These regions receive values close to a probability of roughly 1.0. The difference histogram serves as the basis for calculating the probability (P_h) of the region homogeneity.

$$P_h = \sum \frac{1}{1+i^2} \cdot \frac{f_{diff}}{2.x.y} \tag{5}$$

where x and y are the number of columns and rows in the image, and f_{diff} is the frequency with which the corresponding differences in the two images occur.

The hybrid segmentation module was used as a lightweight preprocessing step to localize tumor regions before radiomic feature extraction. Although adaptive thresholding and region growing are simpler than recent deep learning-based segmentation models, they offer low computational complexity, easier implementation, and better interpretability. In this study, segmentation is not treated as the primary contribution; instead, it supports the extraction of radiomic features such as texture, intensity, shape, border irregularity, wavelet, and asymmetry-based descriptors. Therefore, the proposed segmentation step is designed to provide consistent tumor-region localization for feature extraction rather than to compete with state-of-the-art segmentation networks.

D. Feature Extraction

Several characteristics are derived from the segmented images in this research, including texture features, gradient-based features, intensity-based features, histogram-features, and hybrid shape-based features [48].

1) Intensity-based Features : The statistical and structural aspects of the pixel intensities in an image are described using the intensity-based features. These features capture the distribution of pixel intensities within the tumor region, providing quantitative descriptors such as mean, variance, skewness, and kurtosis of the intensity values.

2) Texture Features: Texture features are used to capture local spatial variations in intensity within the tumor region, which are highly relevant for representing intratumoral heterogeneity. Local Ternary Pattern (LTP) is used to reduce noise-related issues with LBP which is a three-valued ternary code. LTP encodes the local ternary patterns of pixel intensity values in an image. The following formula can be used to determine the LTP features [37].

$$\mathrm{LTP}_{Q,R} = \sum_{z=0}^{Z-1} 2^z \, a(i_z - i_e), a(b_i) = \begin{cases} 1, & b_i \geq Th, \\ 0, & -Th < b_i < Th, \\ -1, & b_i < -Th. \end{cases} \tag{6}$$

Equation (6) states that the neighborhood values will be assigned one of the three values, +1, 0, or -1, based on this comparison. Where R is the circle's radius, Q is the number of neighborhood pixels, i_z and i_e represents the Grey values of the center and neighboring pixels, respectively.

3) Hybrid Shape-based Features: Shape-based features describe the morphology of the segmented tumor by capturing its geometry and boundary structure. Derived from Canny-based edge and contour analysis, these features help distinguish smoother, more regular low-grade tumors from more irregular and infiltrative high-grade tumors [38].

4) Wavelet Transform-based Features: Wavelet transforms decompose an image into different scales and orientations by using a wavelet basis function [39]. The transformation process results in a set of wavelet coefficients that represent image details at various levels of resolution. Utilizing these coefficients features that capture edges, texture, and other aspects of a picture can be extracted.

Let the image sub-band be W_{jk} and jk denote the specific sub-band. The final feature vector will be calculate as

$$f_{jk}(Y) = \iint |W_{jk}(x,y)|^k \, dx \, dy, \qquad Y = 1, 2, 3, \ldots \tag{7}$$

5) Asymmetry index (AI): The asymmetry index (AI) measures the extent to which the segmented tumor departs from bilateral or axial symmetry. It is computed by comparing non-overlapping regions obtained after dividing the tumor around its principal axes. The asymmetric index for glioma grading quantifies irregularities in shape or intensity distribution, aiding in tumor detection [40]. The AI can be calculated as

$$A_I = \frac{A_1 + A_2}{2A_R} \tag{8}$$

where A_1 is the area of the non-overlapped region along the tumors minor axis, A_2 represents an area of the non-overlapped region along the tumors primary axis, A_R is the tumor area Execution. By utilizing the segmented region, the area of the tumor (A_R) can be computed. The lines that cut across the segment's centroid divide the segmented area. After creating two distinct regions, one of the areas is flipped to cause the other two to overlap.

6) Border irregularity: Border irregularity features measure the lack smoothness and complexity of the tumoral border. This property is clinically relevant in the context of glioma MRI, given that high-grade lesions frequently infiltrate and have ill-defined or highly irregular margins compared to otherwise well-circumscribed tumors [41]. Thus, edge-based features help to capture the extent of abruptness or irregularity in tumor shape along its boundary.

We stack all the feature groups into one single feature vector (after extraction) and normalize it before applying to the SIHO enabled LightGBM classifier. Thus the classifier gets a fused representation that integrates complimentary information of tumor density, intra-tumor texture, multi-scale structure, global shape, asymmetry, and edge detail.

E. LightGBM Classifier

In this study, the LightGBM classifier used to grade gliomas, which can handle large datasets efficiently, is based on decision tree methods. Performance and scalability optimization

are the main goals of the development process [42]. The majority of other implementations build trees by adding sequential levels. On the other hand, trees grow their leaves from the bottom up in LightGBM. Moreover, LightGBM uses sorted feature values to determine the optimal split point instead of the popular sorted-based decision tree learning algorithm. Relying on this, LightGBM makes use of an extremely efficient decision tree learning technique based on histograms, which gains substantial advantages in terms of efficiency and memory utilization. As a result, the algorithm runs faster without reducing its high level of accuracy. LightGBM is a high-performance gradient-boosting method that operates quickly and is distributed. Because it uses less memory than other algorithms and trains quickly and effectively. The Exclusive Feature Bundling algorithm is used by LightGBM to manage dataset sparsity. It reduces the number of features while maintaining the most by combining mutually incompatible features in a virtually lossless manner that is instructive.

The LightGBM constructs tree structures iteratively, in each iteration the gradients of the loss function are calculated, and the leaf-wise tree growth strategy selects the leaf with maximum loss. The regularization techniques incorporated in the proposed model minimize the overfitting issues and enhance the generalization ability of the model. Using the previously unseen data, the model's performance will be assessed after training. The hyperparameters of the LightGBM are tuned using the SIHO algorithm.

F. SIHO Algorithm

1) Motivation: The motivation behind developing an SIHO algorithm for glioma grading lies in harnessing the imparting behavior of spuggy [43] and the collaborative hunting traits of coati [44]. Spuggy exhibits dynamic energy accumulation and threat avoidance, while coatis demonstrate intelligent group hunting. This integration in optimization algorithm exhibits improved performance, potentially revolutionizing diagnostic processes in the medical field.

The producers contain a significant amount of energy to provide food directions to other scavengers, which are accountable for identifying food sources. The energy level of the individual is based on the fitness value. When the producer finds any threats it creates a chirp sound as a warning signal. If the warning signal is greater than the safety level the scavengers move to the safe position. Every individual in the group has the potential to become a producer but the individual with a higher energy level would act as the producer. Some famished foragers are inclined to go to the skies in search of sustenance, as a means of obtaining additional vitality. Scavengers follow the producer who can provide the best food. To increase their rate of predation, certain scavengers may compete for food while keeping a careful watch on the producers. The sparrows in the group's center move randomly to remain near one other when a threat is detected, whereas the sparrows on the group's edge quickly move toward the safe location to take up a better position. The suggested SIHO technique was mostly inspired by the simulation of these coatis' natural actions [44]. Overall, the SIHO algorithm leverages the synergy of Spuggy efficient food searching and Coatis' intelligent behaviors to optimize the detection of brain tumors in medical images. By combining these natural behaviors into a computational framework seeks to improve tumor grading precision and effectiveness, providing crucial assistance in the grading of gliomas. The algorithm is a meta-heuristic approach for global optimization, which iteratively updates candidate solutions (Z) based on two main phases: Observation and Attack, or Observation and Escape. The process of Spuggy Interactive hyperparameter Optimization is shown in Algorithm 1. For better presentation and process flow the process is represented in a flowchart presented in Figure 2.

2) Mathematical Formulation: Initialization: The solution's position in the random population is mathematically termed as

$$Z^t = l + q(u - l) - q_1 u \tag{9}$$

where q and q_1 are the random factors $q \in (0, 1)$, the random factor q_1 is described as

$$q_1 = \frac{1}{N} e^{\frac{-t}{t_{\max}}} \in (0, 1) \tag{10}$$

Observation and attack phase ($K(t) < E$): If the prey escape factor $K(t) \in (0, 1)$ is less than the threshold value $E \in (0.5, 1)$, the environment is considered free of threats and the searcher continues to forage for food in the search space. In this situation, the agents remain in exploration mode and update their positions according to the observation and attack behavior of the Spuggy, which can be mathematically expressed as

$$Z^{t+1} = Z^t . \exp\left(\frac{-t}{a_1 t_{\max}}\right) - a_2 e^{\frac{t-1}{t_{\max}}} \tag{11}$$

where α is described as past deterministic factor $s \in (0, 1)$, the hunting tactics are mathematically described as follows

$$Z^{t+1} = Z^t + c\big(Z_g - IZ^t\big) \tag{12}$$

where Z_g represents the global best solution, the fitness probability factor $c \in (0, 1)$ can be calculated as

$$c = \frac{|Fit(Z_g) - Fit(Z_t)|}{|Fit(Z_g) + Fit(Z_t)|} \tag{13}$$

The final equation for the observation and attack phase is derived as

$$Z^{t+1} = 0.5\Big[Z^t . \exp\left(-\frac{t}{a_1 t_{\max}}\right) - a_2 e^{\frac{t-1}{t_{\max}}} + Z^t + c\big(Z_g - IZ^t\big)\Big] \tag{14}$$

The above equation describes that the searchers try to obtain better solutions by the abilities of communication skills and grouping behavior.

Observation and escape phase ($K(t) \geq E$): In this phase, the threat is near the search space the searcher needs to escape from the danger without losing its energy, which is classified into two cases such as safe and unsafe mode.

Subcase (i): Safe Mode ($f_i = f_g$) & $\mathrm{Fit}(Z^t) = \mathrm{Fit}(Z_g)$

This condition shows that the solution inside the pack is aware of the danger, and the position of the searcher is obtained as

$$Z^{t+1} = Z^t + R\left|\frac{Z^t_{\text{worst}}}{\text{Fit}(Z^t) - \text{Fit}_{\text{worst}} + \xi}\right| \tag{15}$$

where ξ is a constant. The distance vector is calculated using the Euclidean distance measure that is expressed as

$$R = \sqrt{(u_2 - u_1)^2 + (v_2 - v_1)^2} \tag{16}$$

where (u_1, v_1) represents the position of worst solutions and (u_2, v_2) denotes the position of the current solution.

Subcase (ii): Unsafe Mode $(f_i \neq f_g)$ & $\text{Fit}(Z^t) \neq \text{Fit}(Z_g)$ The condition shows that the current position of the solution has to be changed because it is at the population's edge and prone to predator attack. To solve this issue, the solution's location is updated using the equation that follows,

$$Z^{t+1} = Z_g + \beta|Z^t - Z_{\text{best}}| \tag{17}$$

where Z_g and Z_{best} represents the global best parameters, β is the step size parameter with mean 0 and variance 1. The solution update equation derived from Coatis is described as follows

$$Z^{t+1} = Z^t + (1 - 2c)\big(lb^{\text{local}} + c(ub^{\text{local}} - lb^{\text{local}})\big) \tag{18}$$

where the upper and lower boundaries are described as $lb^{\text{best}} = \dfrac{lb}{t}$ and $ub^{\text{best}} = \dfrac{ub}{t}$, the final equation for the solution update is expressed as

$$Z^{t+1} = 0.5\Big[Z_g + \beta|Z^t - Z_{\text{best}}| + Z^t + (1 - 2c)\big(lb^{\text{local}} + c(ub^{\text{local}} - lb^{\text{local}})\big)\Big] \tag{19}$$

The equation describes the solution update of searchers to escape from the dangers to make a safe position.

IV. Results and Discussion

This section examines the SIHO-enabled LightGBM model's effectiveness for grading gliomas, evaluating its accuracy and comparing it with other machine learning methods to assess performance.

A. Experimental Setup

Experiments were conducted on the BraTS 2019 dataset (335 cases: 259 HGG, 76 LGG). All data partitioning was performed at the patient level to prevent data leakage. For the primary evaluation, an 80:20 stratified holdout split was applied, yielding 268 training cases (≈213 HGG, ≈55 LGG) and 67 test cases (≈46 HGG, ≈21 LGG), preserving the original 3.4:1 class ratio in both subsets. To assess generalization beyond a single split, stratified k-fold cross-validation was performed across $k = 6, 7, 8, 9$, and 10. In each configuration, the dataset was partitioned into k mutually exclusive patient-level folds; $k-1$ folds were used for training and the remaining fold for evaluation, repeated until every fold served as the test fold. Performance was averaged across all folds. In both evaluation protocols, SIHO-based hyperparameter optimization was applied exclusively to the training partition of each split. The class imbalance between HGG and LGG cases was addressed by setting the LightGBM scale_pos_weight parameter to 3.4, corresponding to the inverse class frequency ratio, thereby assigning greater misclassification cost to the minority LGG class. Model performance is assessed using accuracy, sensitivity, specificity, and F1-score, as these metrics jointly provide a more balanced evaluation under class imbalance and are less susceptible to inflation caused by majority-class dominance.

Algorithm 1 Spuggy Interactive Hyper parameter Optimization

Initialize iteration count $t \leftarrow 0$
Generate initial population $\{Z_i^0\}_{i=1}^N$ uniformly at random within Ω
Evaluate fitness $Fit(Z_i^0)$ for all i by training LightGBM with Z_i^0 and computing the validation metric
Set global best Z_g and worst Z_{worst} solutions according to $Fit(\cdot)$
while $t < t_{max}$ **do**
  for each agent $i = 1, \ldots, N$ **do**
    draw a random number $K \sim U(0, 1)$
    if $K(t) < E$ **then** ▷ Observation and attack phase
      Update the position of agent i using the observation-attack rule as in Eq. (14).
    else ▷ Observation and escape phase
      if $Fit(Z_i^t) = Fit(Z_g)$ **then** ▷ Safe mode
        Update the position using the safe-mode rule as in Eq. (15).
      else ▷ Unsafe mode
        Update the position using the unsafe-mode rule as in Eq. (19).
      end if
    end if
    Project Z_i^{t+1} back onto Ω if any component violates its bounds.
  end for
  Evaluate fitness $Fit(Z_i^{t+1})$ for all agents using the updated hyperparameters.
  Update Z_g (global best) and Z_{worst} based on the new fitness values.
  Set $t \leftarrow t + 1$ and $K(t) = 1 - \frac{t}{t_{\max}}$
end while
return the global best solution Z_g as the optimized LightGBM hyperparameter configuration.

B. Performance Mtrics

The following performance measures are used to assess the SIHO-enabled LightGBM model's performance.

1) Accuracy: Accuracy measures the ratio of correctly classified gliomas into their respective grades with the total predictions.

$$\text{accuracy} = \frac{GL_{tp} + GL_{tn}}{GL_{tp} + GL_{tn} + GL_{fp} + GL_{fn}} \tag{20}$$

2) Sensitivity: The measure of an SIHO-enabled LightGBM model to correctly identify true gliomas among all positive cases

$$\text{Sensitivity} = \frac{GL_{tp}}{GL_{tp} + GL_{fn}} \tag{21}$$

3) Specificity: The measure of SIHO-enabled LightGBM model to correctly identify non gliomas among all negative cases, which can be calculated as

$$\text{Specificity} = \frac{GL_{tn}}{GL_{tn} + GL_{fp}} \tag{22}$$

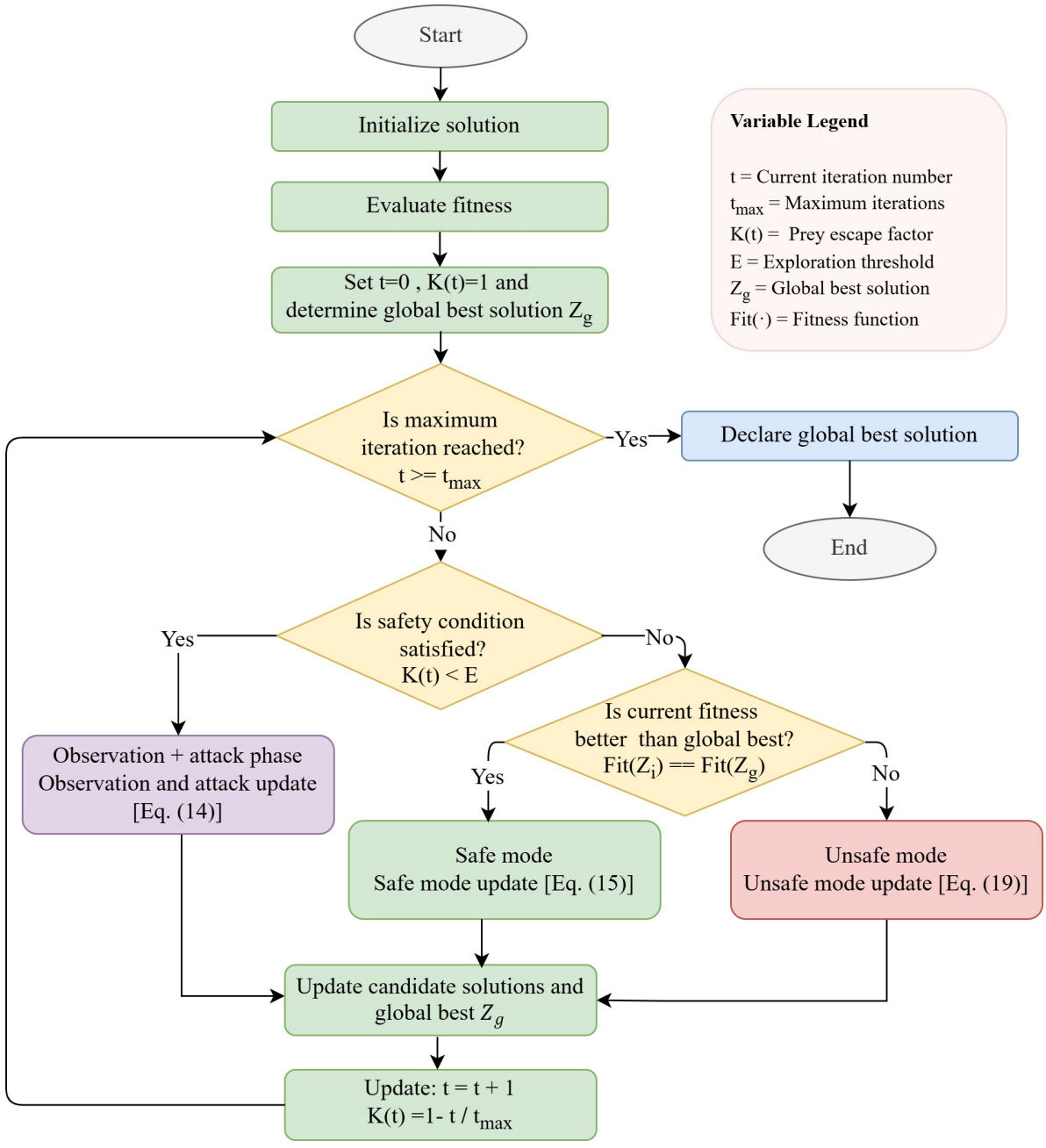


Fig. 2. Flowchart of the proposed SIHO algorithm for LightGBM Hyperparameter optimization

4) F1-score: The F1 score measures the harmonic mean of precision and recall, which can be calculated as

$$F1 = \frac{2 \times \text{precision} \times \text{recall}}{\text{precision} + \text{recall}} \tag{23}$$

C. Performance Analysis

1) Performance Analysis with Training percentage (TP): Figure 3 presents the performance analysis of the SIHO-enabled LightGBM model across various training percentages, specifically 40, 50, 60, 70, and 80. The accuracy of the proposed model, evaluated using TP 80 for epoch values of 20, 40, 60, 80, and 100, is 91.15%, 92.39%, 93.90%, 96.59%, and 95.51%, respectively. Similarly, the model achieves sensitivities of 91.10%, 92.17%, 92.71%, 94.73%, and 94.79% for the corresponding epochs. The specificity attained by the SIHO-LightGBM model for epoch values of 20, 40, 60, 80, and 100 is 91.20%, 92.88%, 96.11%, 96.98%, and 96.28%, respectively. For epochs 20, 40, 60, 80, and 100, the proposed model achieves F1-scores of 89.45%, 89.94%, 93.78%, 95.22%, and 94.24% respectively.

2) Performance Analysis with K-fold: The performance of the proposed SIHO-enabled LightGBM model under k-fold cross-validation is presented in Figure 4, where k was varied as 6, 7, 8, 9, and 10. The model was evaluated using training epochs of 20, 40, 60, 80, and 100, and the

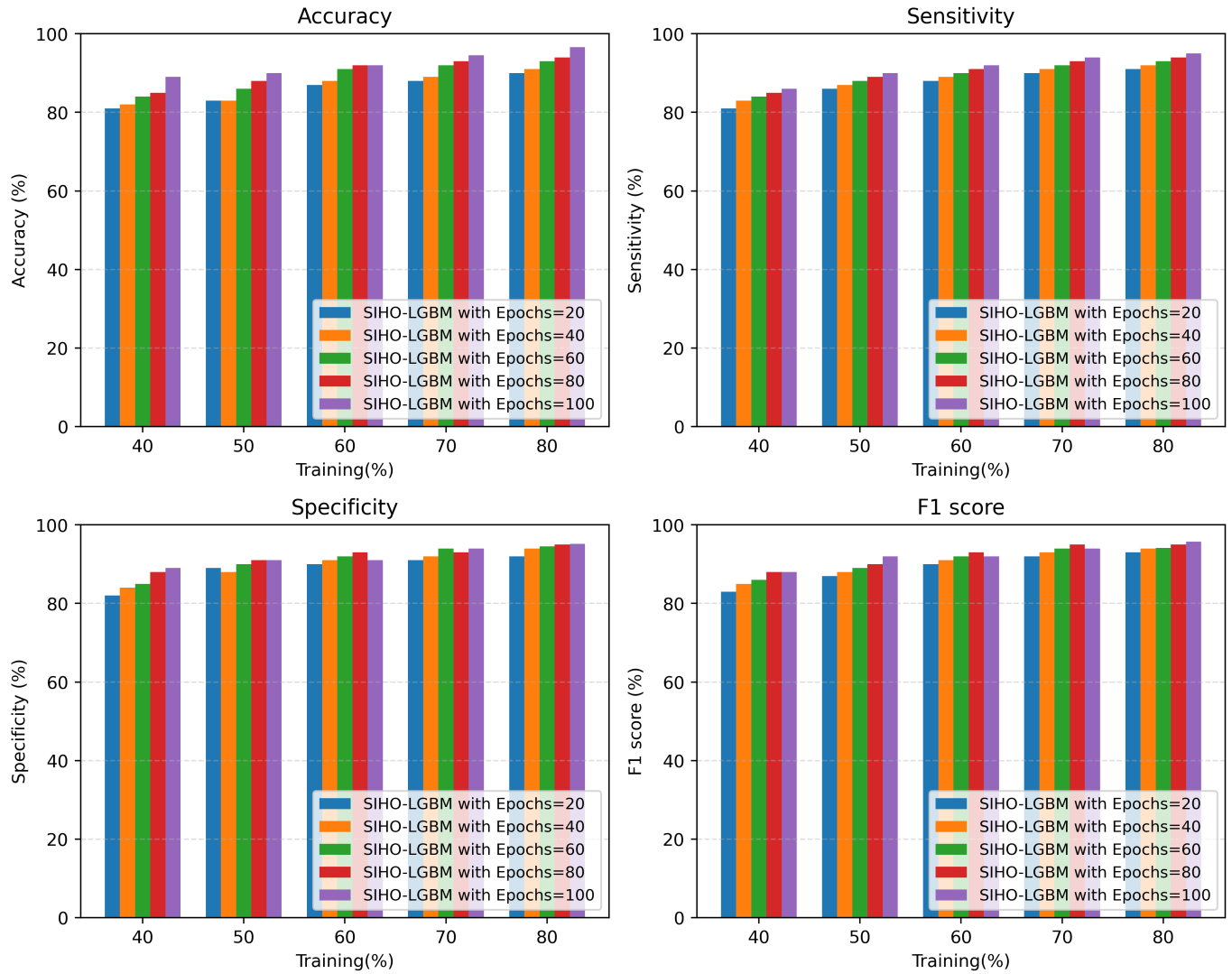


Fig. 3. Internal performance analysis of the proposed SIHO-enabled LightGBM model under different training percentages and epoch values.

reported results represent the average values obtained across all folds for each experimental setting. The average accuracy increased from 91.73% to 96.33% as the number of epochs increased. Similarly, the sensitivity improved from 87.73% to 93.97%, while the specificity increased from 92.28% to 96.98%. The corresponding F1-score also improved from 89.60% to 95.16%. These results indicate that the proposed model maintained stable and strong performance across different fold settings, demonstrating its robustness and reliability under cross-validation.

D. Comparative Methods

The performance of the proposed glioma grading model is compared with the conventional techniques such as KNN [45], VGG19 [47], CNN [36], Deep-CNN [32], LightGBM [42], SSA based LightGBM, and COA based LightGBM.

1) Comparative Analysis with TP: The comparative evaluation of the SIHO enabled LightGBM with the traditional methods such as KNN, VGG19, CNN, Deep-CNN, LightGBM, SSA based LightGBM, and COA based LightGBM with TP 80 is shown in Figure 5 (a). The SIHO enabled LightGBM model attains accuracy of 96.59%, which shows improvement over the classical KNN by 16.30%, VGG19 by 11.85% CNN by 15.14%, Deep-CNN by 10.21%, LightGBM by 8.03%, SSA based LightGBM by 6.02%, and COA based LightGBM by 6.59%.

2) Comparative Analysis with K-fold: Figure 5 (b) compares the SIHO-enabled LightGBM with the traditional methods, including KNN, VGG 19, CNN, Deep-CNN, LightGBM, SSA-based LightGBM, and COA-based LightGBM with k-fold 10. The accuracy of the SIHO-enabled LightGBM model is 96.33%, indicating improvement over the classical KNN by 16.63%, VGG 19 by 10.72% CNN by 15.23%, Deep-CNN by 7.56%, LightGBM by 8.92%, SSA based LightGBM by 8.72%, and COA based LightGBM by 5.17%.

3) AUC-ROC Analysis: The AUC-ROC analysis of the SIHO-enabled LightGBM model is depicted in Figure 6. The ROC curve compares the discriminative performance of all models, showing that each model outperformed random guessing (diagonal line). The SIHO-enabled LightGBM curve

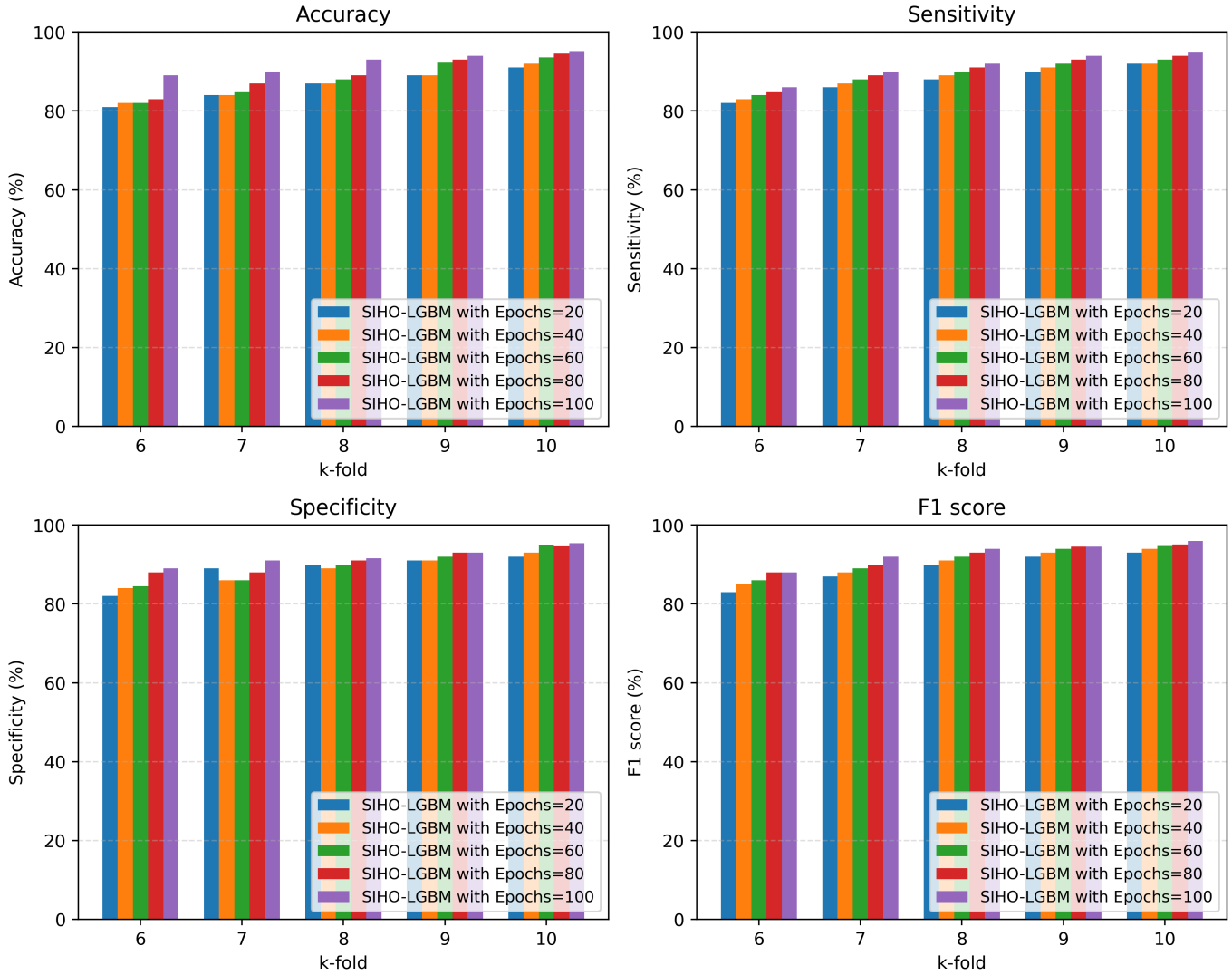


Fig. 4. Internal performance analysis of the proposed SIHO-enabled LightGBM model under different k-fold settings and epoch values.

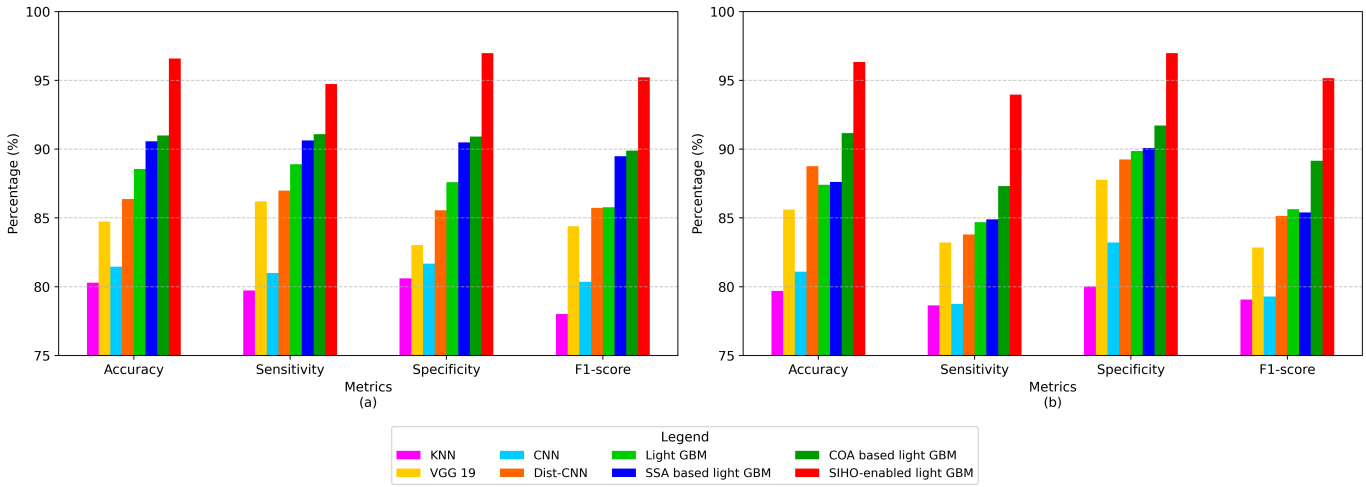


Fig. 5. Comparative performance analysis of Models a) Results with training percentage of 80. b) Results with 10-fold cross validation

dominated the others, indicating the highest AUC-ROC and thus the best overall glioma grading performance.

The consistent upward trend observed in Figs. 3–5 is mainly due to increased training data, repeated SIHO-based hyperparameter optimization, and normalized radiomic features. As the training percentage increases, the classifier learns more representative HGG and LGG feature patterns, reducing false positives and false negatives. Similarly, higher epoch values provide more opportunities for SIHO to refine LightGBM hyperparameters. Since accuracy, sensitivity, specificity, and F1-score are derived from the same prediction outcomes, improvement in class-level predictions can produce similar trends across all metrics. However, these results represent internal validation trends, and external validation is required to confirm their consistency on independent datasets.

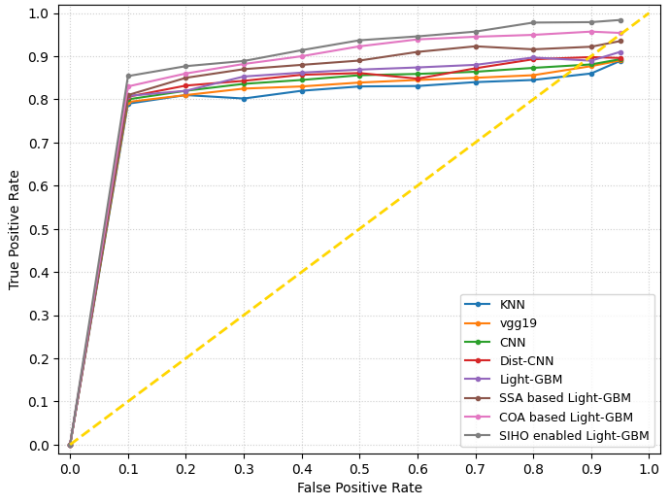


Fig. 6. AUC-ROC analysis for SIHO-enabled LightGBM model

E. Impact of SIHO-Based Hyperparameter Optimization

To clarify the contribution of the proposed SIHO-based hyperparameter optimization, a direct comparison was made between the performances of standard LightGBM and custom-defined SIHO-enabled LightGBM model. This provides the clearest assessment of the effect of incorporating SIHO into the LightGBM framework. The main results shown in Table 1 are kept to help provide a comparative signal, but not treated as a controlled ablation. The results indicate that our proposed LightGBM model with SIHO, outperformed the standard LightGBM under both evaluation settings. For the 80:20 train-test split, it increased from 88.56% to 96.59%, and under 10-Fold Cross Validation it increased from 87.41% to 96.33%. Sensitvity, specificity and F1-score exhibited similar improvements. This result shows that the suggested optimization strategy for SIHO lets the classifier outperform the LightGBM by default due to better hyperparameter tuning. Overall, this analysis indicates that SIHO-based hyperparameter optimization complements the proposed glioma grading model, while the broader comparisons highlighted in Table 1 lend additional strength to the overall framework.

F. Comparative Discussion

The comparative results in Table 1 show that the proposed SIHO-enabled LightGBM model achieved improved glioma grading performance compared with conventional machine learning models, deep learning baselines, standard LightGBM, and other optimization-based LightGBM variants. In the 80:20 train-test setting, the proposed model achieved 96.59% accuracy, while in the 10-fold cross-validation setting, it achieved 96.33% accuracy. Similar performance patterns were observed for sensitivity, specificity, and F1-score, indicating balanced classification between HGG and LGG cases.

The improvement can be mainly attributed to the SIHO-based hyperparameter optimization strategy, which enhances the tuning of LightGBM compared with the non-optimized model. The performance gain over SSA-based LightGBM and COA-based LightGBM further suggests that the proposed SIHO strategy provides an effective optimization mechanism within the evaluated experimental setting. Although the 80:20 split produced slightly higher results than 10-fold cross-validation, the small difference between the two settings indicates relatively stable internal validation performance.

To strengthen the comparative analysis, the proposed method was evaluated against conventional machine learning models, standard LightGBM, optimization-based LightGBM variants, and deep learning baselines, including VGG19, CNN, and Deep-CNN. However, the comparison is limited to the baseline models implemented. Further studies should include comparison with advanced 3D CNN and transformer-based glioma grading networks to provide a broader assessment against stronger deep learning approaches.

Although the results are encouraging, the proposed framework has some limitations. The evaluation was performed only on the BraTS 2019 benchmark dataset and was not validated using independent clinical datasets. Although BraTS 2019 is multi-institutional, it may not fully represent real-world variations in scanner type, acquisition protocol, image quality, and clinical workflow. In addition, the 80:20 test set contains a limited number of cases, and the dataset has an imbalanced distribution between HGG and LGG classes. Although k-fold cross-validation was used for internal validation, statistical robustness remains limited because confidence interval analysis and formal significance testing were not performed. Therefore, the proposed method should currently be considered a controlled experimental decision-support framework rather than a standalone clinical grading system. Future work should include confidence intervals, statistical significance testing, external validation on independent multi-center datasets, and comparison with stronger deep learning-based glioma grading models.

V. Conclusion

This study presented a SIHO-enabled LightGBM framework for automated glioma grading using BraTS 2019 MRI data. This framework integrates FNLM denoising, hybrid tumor segmentation, radiomic feature extraction and SIHO-based hyperparameter optimization to enhance classification accuracy. The derived radiomic features comprised a diversity of tumor

TABLE I
PERFORMANCE COMPARISON OF DIFFERENT METHODS UNDER TP = 80 AND 10-FOLD CROSS-VALIDATION. THE REPORTED VALUES FOR THE 10-FOLD SETTING REPRESENT THE AVERAGE PERFORMANCE ACROSS ALL FOLDS.

Setting	Metric	KNN	VGG19	CNN	Deep-CNN	LightGBM	SSA-based LightGBM	COA-based LightGBM	SIHO-enabled LightGBM
TP 80	Accuracy	80.29	84.74	81.45	86.38	88.56	90.57	91.00	96.59
	Sensitivity	79.73	86.20	81.00	86.98	88.91	90.64	91.09	94.73
	Specificity	80.61	83.03	81.67	85.55	87.60	90.49	90.92	96.98
	F1-score	78.02	84.39	80.35	85.73	85.78	89.49	89.90	95.22
10-fold	Accuracy	79.70	85.61	81.10	88.77	87.41	87.61	91.16	96.33
	Sensitivity	78.64	83.22	78.75	83.79	84.70	84.90	87.31	93.97
	Specificity	80.03	87.77	83.22	89.25	89.87	90.08	91.72	96.98
	F1-score	79.07	82.85	79.29	85.15	85.64	85.40	89.16	95.16

heterogeneity characteristics such as intensity, texture, shape, asymmetry, wavelet and border irregularity. The proposed SIHO-enabled LightGBM model outperformed those baselines under both the 80:20 train-test split setting and the 10-fold cross-validation setting. In the 80:20 evaluation, the model achieved an accuracy of 96.59%, sensitivity of 94.73%, and specificity of 96.98%, performing well with cross-validation too. Based on these results, it can be demonstrated that hyperparameter optimization through SIHO is an essential factor that influences the power of the LightGBM classifier for glioma grading. However, the study was limited to the BraTS 2019 benchmark dataset and was not validated on real-time clinical data. Therefore, the reported results should be interpreted as benchmark-based evidence rather than direct clinical validation. Overall, the proposed method shows promise as a decision-support framework for automated glioma grading, and future work will focus on external clinical validation and broader generalization studies.

REFERENCES

[1] L. Zhao and K. Jia, "Multiscale CNNs for Brain Tumor Segmentation and Diagnosis," Comput Math Methods Med, vol. 2016, no. 1, pp. 1–7, Mar. 2016, doi: 10.1155/2016/8356294.

[2] R. Kumar, A. Gupta, H. S. Arora, G. N. Pandian, and B. Raman, "CGHF: A Computational Decision Support System for Glioma Classification Using Hybrid Radiomics- and Stationary Wavelet-Based Features," IEEE Access, vol. 8, pp. 79440–79458, May 2020, doi: 10.1109/ACCESS.2020.2989193.

[3] D. J. Aum, D. H. Kim, T. L. Beaumont, E. C. Leuthardt, G. P. Dunn, and A. H. Kim, "Molecular and cellular heterogeneity: the hallmark of glioblastoma," Neurosurg Focus, vol. 37, no. 6, Dec. 2014, doi: 10.3171/2014.9.FOCUS14521.

[4] J. M. Lemée, A. Clavreul, and P. Menei, "Intratumoral heterogeneity in glioblastoma: don't forget the peritumoral brain zone," Neuro Oncol, vol. 17, no. 10, pp. 1322–1332, 2015, doi: 10.1093/neuonc/nov119.

[5] D. N. Louis, H. Ohgaki, O. D. Wiestler, et al., "The 2007 WHO classification of tumours of the central nervous system," Acta Neuropathol, vol. 114, no. 2, pp. 97–109, 2007, doi: 10.1007/s00401-007-0243-4.

[6] P. Wesseling and D. Capper, "WHO 2016 Classification of gliomas," Neuropathol Appl Neurobiol, vol. 44, no. 2, pp. 139–150, 2018, doi: 10.1111/nan.12432.

[7] Y. W. Park, P. Vollmuth, M. Foltyn-Dumitru, F. Sahm, S. S. Ahn, J. H. Chang, and S. H. Kim, "The 2021 WHO Classification for Gliomas and Implications on Imaging Diagnosis: Part 1—Key Points of the Fifth Edition and Summary of Imaging Findings on Adult-Type Diffuse Gliomas," J Magn Reson Imaging, vol. 58, pp. 677–689, 2023, doi: 10.1002/jmri.28743.

[8] D. N. Louis, A. Perry, G. Reifenberger, et al., "The 2016 World Health Organization Classification of Tumors of the Central Nervous System: a summary," Acta Neuropathol, vol. 131, no. 6, pp. 803–820, 2016, doi: 10.1007/s00401-016-1545-1.

[9] P. Wesseling, M. van den Bent, and A. Perry, "Oligodendroglioma: pathology, molecular mechanisms and markers," Acta Neuropathol, vol. 129, no. 6, pp. 809–827, 2015, doi: 10.1007/s00401-015-1424-1.

[10] Y. H. Byun and C. K. Park, "Classification and Diagnosis of Adult Glioma: A Scoping Review," Brain & NeuroRehabilitation, vol. 15, no. 3, 2022, doi: 10.12786/bn.2022.15.e23.

[11] Q. Liu, et al., "Treatment-Aware Diffusion Probabilistic Model for Longitudinal MRI Generation and Diffuse Glioma Growth Prediction," IEEE Trans. Med. Imaging, vol. 44, no. 6, pp. 2449–2462, 2025, doi: 10.1109/TMI.2025.3533038.

[12] S. S. Yathirajam and S. Gutta, "Efficient glioma grade prediction using learned features extracted from convolutional neural networks," J Med Artif Intell, vol. 7, no. 2, 2024, doi: 10.21037/jmai-23-161.

[13] H. K. Lakshmikanth, K. Rajagopal, P. Mohan Shenoy, and S. Mustaffa, "First-pass CT-perfusion in differentiating primary extra-axial brain tumours: Added value of MTT and TTP in characterisation beyond CBV and CBF," The Egyptian Journal of Radiology and Nuclear Medicine, vol. 49, no.3, pp. 693–700, 2018, doi: 10.1016/j.ejrnm.2018.05.008.

[14] T. B. Shaw, R. L. Jeffree, P. Thomas, et al., "Diagnostic performance of 18F-fluorodeoxyglucose positron emission tomography in the evaluation of glioma," J Med Imaging Radiat Oncol, vol. 63, no. 5, pp. 650–656, doi: 10.1111/1754-9485.12929.

[15] M. D. Anderson, R. R. Colen, and I. W. Tremont-Lukats, "Imaging mimics of primary malignant tumors of the central nervous system (CNS)," Curr Oncol Rep, vol. 16, no. 8, doi: 10.1007/s11912-014-0399-8.

[16] N. Upadhyay, and A. D. Waldman, "Conventional MRI evaluation of gliomas," Br J Radiol, 84 Spec No 2(Spec Iss 2), pp. S107-S111, 2011, doi: 10.1259/bjr/65711810.

[17] J. G. Suárez-García, J. M. Hernández-López, E. Moreno-Barbosa, and B. de Celis-Alonso, "A simple model for glioma grading based on texture analysis applied to conventional brain MRI," PLoS ONE, vol. 15, no. 5, 2020, doi: 10.1371/journal.pone.0228972.

[18] J. Saini, P. K. Gupta, P. Sahoo, et al., "Differentiation of grade II/III and grade IV glioma by combining "T1 contrast-enhanced brain perfusion imaging and susceptibility-weighted quantitative imaging," Neuroradiology, vol. 60, pp. 43–50, doi: 10.1007/s00234-017-1942-8.

[19] W. Deng, W. Xiao, H. Deng, and J. Liu, "MRI Brain Tumor Segmentation With Region Growing Method Based On The Gradients And Variances Along And Inside Of The Boundary Curve," Proceedings - 2010 3rd International Conference on Biomedical Engineering and Informatics, BMEI 2010, vol. 1, pp. 393–396, 2010, doi: 10.1109/BMEI.2010.5639536.

[20] W. Wang, Y. Zhao, L. Teng, et al., "Neuropathologist-level integrated classification of adult-type diffuse gliomas using deep learning from whole-slide pathological images," Nat Commun, vol. 14, 2023, doi: 10.1038/s41467-023-41195-9.

[21] R. C. Joshi, R. Mishra, P. Gandhi, V. K. Pathak, R. Burget, and M. K. Dutta, "Ensemble based machine learning approach for prediction of glioma and multi-grade classification," Comput Biol Med, vol. 137, 2021, doi: 10.1016/j.compbiomed.2021.104829.
[22] V. Z. Miloushev, D. S. Chow, and C. G. Filippi, "Meta-Analysis of Diffusion Metrics for the Prediction of Tumor Grade in Gliomas," American Journal of Neuroradiology, vol. 36, no. 2, pp. 302–308, 2015, doi: 10.3174/ajnr.A4097.
[23] D. Lu, and Q. Weng, "A survey of image classification methods and techniques for improving classification performance," International Journal of Remote Sensing, vol. 28, no. 5, pp. 823–870, 2007, doi: 10.1080/01431160600746456.
[24] A. Arisawa, Y. Watanabe, H. Tanaka, et al., "Comparative study of pulsed-continuous arterial spin labeling and dynamic susceptibility contrast imaging by histogram analysis in evaluation of glial tumors," Neuroradiology, vol. 60, pp. 599–608, 2018, doi: 10.1007/s00234-018-2024-2.
[25] T. Xie, X. Chen, J. Fang, et al., "Textural features of dynamic contrast-enhanced MRI derived model-free and model-based parameter maps in glioma grading," J Magn Reson Imaging, vol. 47, no. 4, pp. 1099–1111, 2018, doi: 10.1002/jmri.25835.
[26] J. A. Guzmán-De-Villoria, J. M. Mateos-Pérez, P. Fernández-García, E. Castro, and M. Desco, "Added value of advanced over conventional magnetic resonance imaging in grading gliomas and other primary brain tumors," Cancer Imaging, vol. 14, no. 1, 2014, doi: 10.1186/s40644-014-0035-8.
[27] S. Rathore, T. Niazi, M. A. Iftikhar, and A. Chaddad, "Glioma Grading via Analysis of Digital Pathology Images Using Machine Learning," Cancers, vol. 12, no. 3, 2020, doi: 10.3390/cancers12030578.
[28] A. Raza, H. Ayub, J. A. Khan, I. Ahmad, A. S. Salama, Y. I. Daradkeh, D. Javeed, A. Ur Rehman, and H. Hamam, "A Hybrid Deep Learning-Based Approach for Brain Tumor Classification," Electronics, vol. 11, no. 7, 2022, doi: 10.3390/electronics11071146.
[29] S. Im, J. Hyeon, E. Rha, J. Lee, Choi H-J, Y. Jung, and Kim T-J, "Classification of Diffuse Glioma Subtype from Clinical-Grade Pathological Images Using Deep Transfer Learning," Sensors, vol. 21, no. 10, 2021, doi: 10.3390/s21103500.
[30] B. Niu, C. Liang, Y. Lu, M. Zhao, Q. Chen, Y. Zhang, L. Zheng, and K. C. Chou, "Glioma stages prediction based on machine learning algorithm combined with protein-protein interaction networks," Genomics, vol. 112, no. 1, pp. 837–847, 2020, doi: 10.1016/j.ygeno.2019.05.024.
[31] M. Rizwan, A. Shabbir, A. R. Javed, M. Shabbir, T. Baker, and D. Al-Jumeily Obe, "Brain Tumor and Glioma Grade Classification Using Gaussian Convolutional Neural Network," IEEE Access, vol. 10, pp. 29731–29740, 2022, doi: 10.1109/ACCESS.2022.3153108.
[32] H. Mzoughi, I. Njeh, A. Wali, et al., "Deep Multi-Scale 3D Convolutional Neural Network (CNN) for MRI Gliomas Brain Tumor Classification," J Digit Imaging, vol. 33, pp. 903–915, 2020, doi: 10.1007/s10278-020-00347-9.
[33] BraTS 2019 dataset. http://www.med.upenn.edu/cbica/brats2019/data.html (accessed on October 2023).
[34] H. Kim, S. Lim, M. Park, K. Kim, S. H. Kang, and Y. Lee, "Optimization of Fast Non-Local Means Noise Reduction Algorithm Parameter in Computed Tomographic Phantom Images Using 3D Printing Technology," Diagnostics (Basel), vol. 14, no. 15, 2024, doi: 10.3390/diagnostics14151589.
[35] Kang S-H, S. Lee, and Y. Lee, "Experimental study of noise level optimization in brain single-photon emission computed tomography images using non-local means approach with various reconstruction methods," Nuclear Engineering and Technology, vol. 55, no.5, pp. 1527–1532, 2023, doi: 10.1016/j.net.2023.01.013.
[36] Özkaya Ç, and Sağiroğlu Ş, "Glioma Grade Classification Using CNNs and Segmentation with an Adaptive Approach Using Histogram Features in Brain MRIs," IEEE Access, vol. 11, pp. 52275–52287, 2023, doi: 10.1109/ACCESS.2023.3273532.
[37] W. Muzaffar, et al., "Gabor Contrast Patterns: A Novel Framework to Extract Features from Texture Images," IEEE Access, vol. 11, pp. 60324–60334, 2023, doi: 10.1109/ACCESS.2023.3280053.
[38] H. Zhao, G. Qin, and X. Wang, "Improvement of canny algorithm based on pavement edge detection," International Congress on Image and Signal Processing, vol. 2, pp. 964–967, 2010, doi: 10.1109/CISP.2010.5646923.
[39] A. Dede, H. Nunoo-Mensah, E. K. Akowuah, K. O. Boateng, P. E. Adjei, F. A. Acheampong, I. Acquah, and J. J. Kponyo, "Wavelet-Based Feature Extraction for Efficient High-Resolution Image Classification," Engineering Reports, vol. 7, 2025, doi: 10.1002/eng2.70027.
[40] G. Gihr, D. Horvath-Rizea, P. Kohlhof-Meinecke, O. Ganslandt, H. Henkes, W. Härtig, A. Donitza, M. Skalej, and S. Schob, "Diffusion Weighted Imaging in Gliomas: A Histogram-Based Approach for Tumor Characterization," Cancers, vol. 14, no. 14, 2022, doi: 10.3390/cancers14143393.
[41] J. Jaworek-Korjakowska, and R. Tadeusiewicz, "Determination of border irregularity in dermoscopic color images of pigmented skin lesions," Annu Int Conf IEEE Eng Med Biol Soc, pp. 6459–6462, 2014, doi: 10.1109/EMBC.2014.6945107.
[42] A. Mohammed, S. Hussein, et al., "Brain Tumor Classification using hybrid algorithms (VGG19) and Light(GBM)," Neuroquantology, vol. 20, no. 11, pp. 6562–6578, 2022, doi: 10.14704/NQ.2022.20.11.NQ66655.
[43] T. Liu, Z. Yuan, L. Wu, and B. Badami, "An optimal brain tumor detection by convolutional neural network and Enhanced Sparrow Search Algorithm," Proc Inst Mech Eng H, vol. 235, no. 4, pp. 459–469, 2021, doi: 10.1177/0954411920987964.
[44] M. Dehghani, Z. Montazeri, E. Trojovska, and P. Trojovsky, "Coati Optimization Algorithm: A new bio-inspired metaheuristic algorithm for solving optimization problems," Knowledge-Based Systems, vol. 259, 2023, doi: 10.1016/j.knosys.2022.110011.
[45] S. Saeed, A. Abdullah, N. Z. Jhanjhi, M. Naqvi, and A. Nayyar, "New techniques for efficiently k-NN algorithm for brain tumor detection," Multimedia Tools Appl, vol. 18, no. 13, pp. 18595–18616, 2022, doi: 10.1007/s11042-022-12271-x.
[46] Z. Yang, A. Zamarud, N. J. Marianayagam, D. J. Park, et al., "Deep learning-based overall survival prediction in patients with glioblastoma: An automatic end-to-end workflow using pre-resection basic structural multiparametric MRIs," Computers in Biology and Medicine, vol. 185, 2025, doi: 10.1016/j.compbiomed.2024.109436.
[47] S. Arlis, M. Putra, and M. Yanto, "Effectiveness of VGG19 in deep learning for brain tumor detection," Indonesian Journal of Electrical Engineering and Computer Science, vol. 35, 2024, doi: 10.11591/ijeecs.v35.i2.pp1210-1218.
[48] N. Hasan, M. F. Ahmed, M. A. Nasif, M. R. Haq, and M. Rahman, "Hybrid Feature Extraction Approach for Robust Brain Tumor Classification: HOG, GLCM, and Artificial Neural Network," 2024 6th International Conference on Electrical Engineering and Information & Communication Technology (ICEEICT), pp. 1292–1297, 2024, doi: 10.1109/ICEEICT62016.2024.10534587.
[49] A. Verma, and A. K. Yadav, "FusionNet: Dual input feature fusion network with ensemble based filter feature selection for enhanced brain tumor classification," Brain Research, vol. 1852, 2025, doi: 10.1016/j.brainres.2025.149507.



Thota Deepa a full-time research scholar in the Department of Computer Science and Engineering at Sri Venkateswara University, Tirupathi, India. Commenced her academic journey with a B.Tech in 2005 and advanced her qualifications with an M.Tech in 2012. After contributing 7 years as an assistant professor, she has shifted her scholarly pursuits to rigorous research since 2019, focusing on cutting-edge areas such as Artificial Intelligence, Neural Networks, Machine Learning, and Deep Learning.



Ch D V Subba Rao is currently with Computer Science and Engineering Department at Sri Venkateswara University, Tirupati, Andhra Pradesh. He began his career in 1992 at SV University and previously taught at REC Warangal (now NIT Warangal). Prof. Rao has published over 78 papers in reputed international journals. He has guided 7 PhD scholars and 41 M.Tech theses, authored 3 textbooks, and holds 2 patents. At present he is supervising the work of 7 PhD scholars. He is associated with IETE and IE (India), and a Senior Member of the Computer Society of India. His research interests include Distributed Systems, Wireless Networks, Data Engineering, and Cloud Computing.